Resources, Conservation & Recycling 229 (2026) 108846

Contents lists available at ScienceDirect

Resources, Conservation & Recycling

journal homepage: www.sciencedirect.com/journal/resources-conservation-and-recycling

Full length article

Intrinsic controls on the kinetics of calcium extraction from crystalline slags: Implications on CO_2 mineralization

Erika La Plante [a,1,*], Adriano Leão [b,c,1], Micah Bob [a], Yi-Hsuan Hsiao [c], Owen Daily [b,c], Gwenn Le Saout [d], Laurent Pilon [e], Gaurav N. Sant [b,c,f,g]

[a] Department of Materials Science and Engineering, University of California, Davis, CA 95616, USA
[b] Institute for Carbon Management, University of California, Los Angeles, CA 90095, USA
[c] Department of Civil and Environmental Engineering, University of California, Los Angeles, CA 90095, USA
[d] Laboratoire de Mécanique et Génie Civil (LMGC), IMT Mines Alès, Université de Montpellier, CNRS, Alès, France
[e] Department of Mechanical and Aerospace Engineering, University of California, Los Angeles, CA 90095, USA
[f] Department of Materials Science and Engineering, University of California, Los Angeles, CA 90095, USA
[g] California Nanosystems Institute, University of California, Los Angeles, CA 90095, USA

ARTICLE INFO

Keywords:
Dissolution
Time-dependent rate
Mineralogy

ABSTRACT

Slags are a potent source of Ca^{2+} cations for CO_2 mineralization reactions. Although studies have been performed to characterize the effects of processing conditions on slag dissolution rates, systematic analyses of the mineralogical controls that affect multicomponent dissolution kinetics and associated Ca release remain sparse. Here, the aqueous Ca extractability of six different types of crystalline slags: electric arc furnace (EAF), basic oxygen furnace (BOF), air-cooled blast furnace (ac-BF), co-mingled electric arc furnace (cm-EAF), stainless steel (SS), and ladle slag (LS), was quantified for varying particle size, solid-to-liquid ratio, reagent, temperature, and pH conditions. We show that the evolution of dissolved Ca over time can be described by power relationships, indicating temporally decreasing rates of Ca release, wherein the (apparent) rate constants describe extrinsic controls on kinetics. In addition, we clarified that Ca release kinetics in crystalline slags is directly related to its mineralogy, particularly the amounts of Ca-containing silicate, aluminate, carbonate, and oxide minerals, which further have distinct pH-dependent reactivities. The degree of polymerization of Ca silicates, which can be correlated with the slag's bulk chemical composition, exerts significant control over Ca extraction rates. The outcomes of this study can be applied to optimize, for instance, mineralization carbonation processes involving the use of crystalline Ca-rich alkaline solids in various leaching environments.

1. Introduction

Iron and steel are vital global commodities (Kumar and Kumar, 2015) that are associated with byproducts including slag and CO_2 emissions (International Energy Agency, 2021; Olmez et al., 2016). In response to growing environmental concerns (Leão et al., 2023; Leão et al., 2020; Vogl et al., 2021), one approach toward mitigating global CO_2 atmospheric concentrations is its mineralization as relatively insoluble carbonate minerals such as calcium and magnesium carbonates (Huijgen and Comans, 2003; Bobicki et al., 2012). In this process, CO_2 is reacted with an alkaline solid in an aqueous medium. The alkaline solid provides the cations Ca^{2+} and Mg^{2+} that react with CO_3^{2-} ions in the water, from dissolved CO_2, to form carbonates (DiGiovanni et al., 2024; Li et al., 2025). Industrial alkaline byproducts such as slag and fly ash have an estimated global annual production of ~7-to-17 Gt, corresponding to a significant carbon sequestration potential of ~200–330 Mt (Renforth et al., 2011; Kirchofer et al., 2013). While internal recycling (Dutta and Chokshi, 2020) and incorporation into construction materials (Grubeša and Barišic, 2021) have been increasingly adopted, at least 40% of all slag generated is disposed in landfills (Moon et al., 2024; Guo et al., 2018). Carbonation can be achieved through a single, direct process in which CO_2 is reacted with the alkaline solid to form calcite in solution or on solid surfaces (Huijgen and Comans, 2005; Montes-Hernandez et al., 2009), or by a sequential process involving an initial

* Corresponding author.
E-mail address: eclaplante@ucdavis.edu (E. La Plante).
[1] Both authors contributed equally to this work.

https://doi.org/10.1016/j.resconrec.2026.108846
Received 28 May 2025; Received in revised form 31 January 2026; Accepted 4 February 2026
Available online 11 February 2026

step of solid dissolution, followed by carbonate precipitation in a separate reactor (Chang et al., 2013; Hosseini et al., 2014). In both of these processes, the degree of carbonation is limited by factors including the amount of Ca from the solid that is available for carbonation. This has been a key driver of enhanced slag dissolution research (Li et al., 2022; Wang et al., 2021). Further, in direct carbonation of slags, it has been suggested that dissolution of the slag, and not the precipitation of calcite, is the rate-determining step for the overall reaction, posing a key challenge to practical application at scale (Moon et al., 2024; Huijgen and Comans, 2005).

From the perspective of using alkaline solids for carbonation, it is essential to understand the controls on dissolution kinetics under different processing conditions. Hence, much of the literature in slag leaching kinetics has been motivated towards optimization of CO_2 mineralization processes (Lekakh et al., 2008), for both pure synthesized minerals contained in slags (Zhao et al., 2019; Zhao et al., 2020; Engström et al., 2013; Mei et al., 2022) and as-produced slags (Bobicki et al., 2012; Zhang et al., 2013; Doucet, 2010; Ragipani et al., 2020; Kokko et al., 2024). The effects of processing conditions such as temperature, pH, liquid-to-solid ratio, and specific surface area have been explored, revealing that increasing temperature and surface area, and decreasing pH are all favorable for Ca extraction, as typical for common rock-forming minerals (Lekakh et al., 2008). Much of this previous work on slag leaching kinetics has focused on fitting various rate kinetic models from which the dissolution or leaching mechanism can be inferred (Lekakh et al., 2008; Nikolić et al., 2016). Models such as the nucleation-based Avrami model (Franke et al., 1987; Hulbert, 1970; Christian, 2002), and the shrinking core model (Yagi and Kunii, 1955; Gbor and Jia, 2004) are among those that have been most widely used. Although this approach has provided valuable insight into possible reaction mechanisms, such interpretations are limited by the various assumptions employed in the derivation of each model and may not always be appropriate for the system investigated. The selection of the appropriate model is typically based on a goodness-of-fit parameter (i.e., R^2 value) that is based on curve fitting of a limited number of data points. In some cases, the use of kinetic rate laws is further limited by a lack of direct evidence supporting the proposed mechanisms. Finally, the physical significance of empirically determined apparent rate constants and reaction orders is unclear. Hence, alternative approaches that are able to more directly explain the observed rates are needed.

Although some types of slags such as ground granulated blast furnace slag treated via rapid water-quenching (Europäische Kommission, 2013) find use as supplementary cementitious material, other types such as slowly cooled crystalline slags are disposed of as a reject stream due to their generally low reactivity (Teo et al., 2020). If the size fraction of these slags is not suitable for use as a mineral aggregate in concrete, they are often discarded (Grubeša and Barišic, 2021). Therefore, this study focuses on slags that are predominantly crystalline, which are composed primarily of silicates, oxides, and aluminates of Ca, Mg, and Fe, in varying proportions. These minerals have distinct reactivities in different aqueous environments resulting in distinct reactivities of the slags. It has been demonstrated previously, e.g., using solubility calculations, that the extent of metal release is controlled by the solubility of minerals initially present in the slags, or of the secondary phases that form in solution (Huijgen and Comans, 2006; De Windt et al., 2011). Here, we show how Ca extractability is systematically related to the mineralogy and composition of distinct types of slags.

This study thus demonstrates the factors controlling Ca release kinetics, both chemical and mineralogical, and provides guidance in optimizing leaching conditions such as pH, solid-to-liquid ratio (S:L), and the type of alkaline solids used as feedstock in carbonation processes. To do so, we characterized the dissolution kinetics of different slags, each with its distinct mineralogical assemblage, chemical composition and total Ca content, and degree of crystallinity, under different processing conditions. The rate and extent of Ca release from different types of slags were quantified by measuring the aqueous compositions of reacted solutions over time. Generic rate equations were fitted to the experimental data obtained under varying temperatures, particle size, S:L, and pH, while rate constants were compared and rationalized in terms of the slag's properties. Additional insights, particularly into secondary precipitation, were obtained from thermodynamic calculations of the solution speciation and from high-solid-loading experiments in acid, targeting high rates and extents of Ca mobilization to effect large-scale CO_2 mineralization applications.

2. Materials and methods

2.1. Slag characterization and sample preparation

Six unique crystalline slag types were supplied by TMS International including (1) electric arc furnace (EAF), (2) basic oxygen furnace (BOF), (3) air-cooled blast furnace (ac-BF), (4) co-mingled electric arc furnace (cm-EAF), which is a mixture of EAF and ladle slag, (5) stainless steel (SS) and (6) ladle slag (LS) (**Figure S1**). Air-cooled blast furnace slag is a by-product of iron production, in which the slag is slowly cooled forming crystalline components, whereas BOF, EAF, SS, and LS are obtained from steel production (Yildirim and Prezzi, 2011; Piatak et al., 2015). EAF and BOF slags are steel furnace slags produced when iron and/or scrap metals are oxidized either by applying an electric current or by adding large amounts of pure oxygen, respectively. Ladle slag is produced by further refining molten steel from BOF or EAF slags. These slags are industrially relevant, encompassing a wide range of processing history and mineralogical and compositional diversity.

The slag samples were air-dried and then ground using a ball mill for 40 min. The ground slag was then sieved in series to separate the different particle size fractions ranging from <38 μm to 150–600 μm. The <38 μm fraction was ground manually using an agate mortar and pestle to produce a particle distribution featuring a median diameter, d_{50} ~5 μm. The effect of particle size on dissolution kinetics was investigated for EAF slag. To determine the effect of the solution conditions (e.g., temperature, pH, stirring) on dissolution rate, the 38–53 μm size fraction was used for suitable comparison among different slags. To determine the particle size distributions (PSD) (Fig. 1a and b), particle size analysis was performed using light scattering using a LS13–320 Beckman Coulter static light scattering analyzer. Slag samples were suspended in isopropanol and were sonicated for about 2 min immediately prior to the measurements. Three replicates were obtained for each sample. The particle size fractions correspond to specific surface areas given in **Table S1**, assuming that the particles were spherical. The specific surface areas were taken as the average of three PSD measurements. The relative standard deviation in the average specific surface area of the 38–53 μm size fraction of the different slags was 0.13.

The chemical compositions in mass % of simple oxides of the various slags were measured by X-ray fluorescence (XRF) and are shown in Fig. 1c. The slags were dominantly composed of Ca (32–49 mass % oxide), followed by Si (13–32%), Fe (5–31%), Mg (6–9%), and Al (2–11%), typical for the specific slag types considered (Yildirim and Prezzi, 2011). Notably, blast furnace slag, which is obtained from iron production, had significantly higher Si than the steel slags.

Powdered slags were dried in air at ~45 °C and also analyzed by using X-ray diffraction (XRD) to assess their mineralogy. Analysis of XRD data reveals the presence of various Fe and Mg oxides, Ca and Mg silicates, Ca aluminate, and Fe and Mg hydroxides. The compositional complexity of the solid precludes a fully quantitative analysis of the XRD data; hence, a semi-quantitative analysis is presented herein (see **Table S2**).

Petrographic analysis. Sections having thicknesses of 30 μm of the as-received slag samples were prepared by Wagner Petrographic and viewed under plane- and cross-polarized light using a Leica DM750P polarizing microscope, for characterization of mineralogy and texture, and to supplement the XRD data.

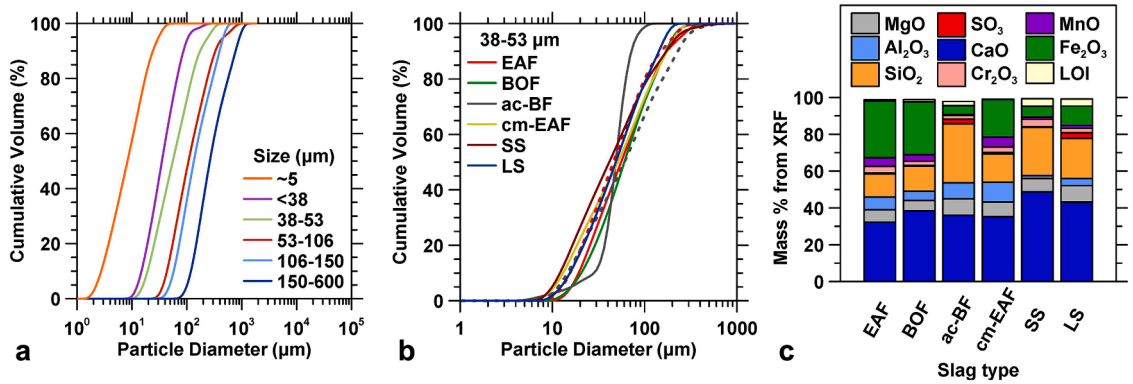

Fig. 1. Size distributions of fractionated particles for **(a)** electric arc furnace (EAF) slag showing the following fractions: ~5, <38, 38–53, 53–106, 106–150, and 150–600 μm, corresponding to median particle diameters d_{50}, and for **(b)** 6 types of slags for the 38–53 μm size fraction. The dashed lines indicate particle size distributions from repeat sample preparation. **(c)** Chemical composition of slags in mass % of oxide, obtained from X-ray fluorescence (XRF).

2.2. Batch experiments

A total of 100 experiments were conducted. In the batch leaching experiments, powdered slag samples were reacted with 100 mL of various aqueous solutions. The reaction solutions were prepared by adding ACS reagent grade chemicals to ~18 MΩ·cm deionized (DI) water. The sampled leachates were filtered through 0.20 μm nylon membranes, and then diluted immediately in 5% nitric acid (HNO_3) matrix prior to refrigeration. Elemental analysis was carried out using a Perkin Elmer Avio 200 inductively coupled plasma–optical emission spectrometer (ICP-OES), with calibration standards prepared from concentrated (1000 ppm) standards from Inorganic Ventures. Instrument calibrations were performed using solutions containing 0, 0.1, 1, 10, 30, and 60 ppm of the elements of interest.

For the experiments at solid-to-liquid mass ratio (S:L) of 1:100, after 0, 1, 3, 6, 24, 72, and 168 h of reaction, the reacted solution was sampled (~3 mL) for analysis of total dissolved Ca, Mg, Si, Fe, Al, Mn, and Na concentrations. The elemental concentrations were corrected for the volume reduction resulting from each sampling interval. The experiments were conducted in different solutions such as pure DI water and in the presence of organic reagents (acetic acid and EDTA), at 25 ± 0.2°C, 45 ± 0.2°C, and 90 ± 3°C using temperature-controlled environmental chambers, and under static conditions, or at ambient temperature (~23°C) under stirred conditions using a magnetic stir bar. The high S:L experiments (S:L of 1:10) were performed using the 106–150 μm particle size fraction of the ac-BF and BOF slags. Dissolution was carried out for 1 hour at ambient temperature and under stirred and pH-controlled condition (i.e., buffered at a fixed pH using 5% HNO_3). The reaction solution was sampled after 0.5, 1, 2, 5, 10, 20, 30, 45, and 60 min.

3. Results and discussion

3.1. Temporally evolving rates of Ca release and the effect of particle size

Commonly applied models for heterogeneous leaching and dissolution reactions in slags include the shrinking core model (SCM) and the Avrami model (Dri et al., 2013; Pecina et al., 2008). We note that the shrinking core model did not successfully fit our kinetic data. The nucleation-based Avrami model is given by: $X = 1 - e^{-kt^{\alpha}}$, where X is the fraction of the reactant reacted at time, t, k is the reaction rate constant, and α is the reaction order typically assumed to contain information about the reaction mechanism and is material-dependent but independent of the process conditions. Although reasonable fits were obtained using this model, the values of k and α exhibited trends that were not consistent with the assumptions of the model. Instead of the previously mentioned models, the fraction of Ca reacted, X_{Ca}, follows a power law dependence as a function of time, given by:

$$X_{Ca} = \frac{m_{Ca,\,t}}{m_{Ca,\,t_0}} = kt^{\alpha} \quad (1)$$

where k is the apparent rate constant and α is the apparent reaction order while $m_{Ca,t}$ and $m_{Ca,\,t_0}$ (mg) are the total mass of Ca dissolved in the solution at time t (h) and the initial mass of Ca in the solid, respectively. Here, k represents the magnitude of Ca release, reflecting the combined influences of multiple physical and chemical factors such as reactive surface area, mineralogy, solution chemistry, and temperature, with higher values indicating faster initial dissolution, whereas α describes how Ca release scales with time; values of 1 suggest linear, reaction-controlled behavior, whereas <1 indicates a decreasing rate, which could be related to transport or surface site limitations. This equation can be linearized to $\ln X_{Ca} = \ln k + \alpha \ln t$ as herein fitted to the data. Fitting of the data was carried out as follows. Initial fitting of both α and k were performed for each data set. Data points featuring a decrease in aqueous Ca concentration and X_{Ca} as time t increases were excluded as they indicate substantial precipitation of Ca-containing phases from the liquid solution. The data were then re-fitted using a constant average α for comparability among the different slag types and particle sizes (Fig. 2a and b).

This general power law can be applied to heterogeneous systems undergoing 'aging', indicated by an apparent temporal decrease in dissolution rate. This behavior may originate from several processes including a decrease in total surface area, a decrease in the reactive surface area, or precipitation of new phases hindering the access of reactant to the dissolving solid (Reeves and Rothman, 2013). This behavior can also be explained using a distributed reactivity model, describing parallel reactions occurring simultaneously but with different rates. Here, as the fastest reactions reached completion, the overall rate of Ca release decreased with time. At longer times, only the slowest reactions persisted, resulting in a much slower rate. This was analogous to a decrease in the number of active surface sites, which may not be proportional to the total surface area, over time as the reaction proceeds. This is likely given that the slags are composed of several minerals, each having a distinct reactivity. Finally, the apparent decrease in rates as a function of time (in power law terms) could also result from the precipitation of secondary phases. The latter can either decrease the dissolution rates directly by the formation of films or apparently by the sequestration of aqueous Ca into the secondary phase, thus reducing aqueous Ca concentrations.

In minerals, the geometrical surface area has been previously shown to better correlate with dissolution rates and not the evolving BET surface area (Gautier et al., 2001). This was attributed to the walls of etch pits that form during dissolution, and which significantly contribute to the BET surface area, as being relatively unreactive. Fig. 2 shows the effect of particle size and specific surface area on the rate constant for

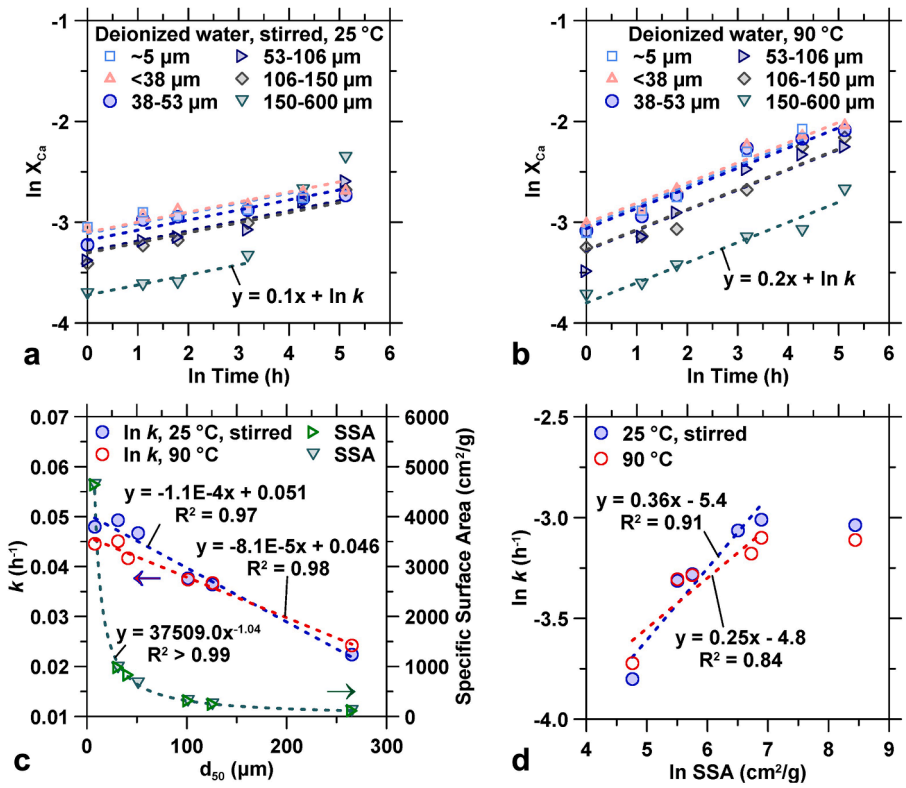

Fig. 2. **(a), (b)** Plots of natural logarithm of Ca reacted, ln X_{Ca}, as a function of natural logarithm of time for the EAF slag. The linear relationship between the two variables indicates a power law dependence of Ca release with time. The trend lines obtained for the 25°C (with stirring) and 90°C (with no stirring) data are similar; the apparent reaction orders are 0.1 and 0.2, respectively. **(c)** The median particle diameter, d_{50}, is related to the specific surface area, as shown, and is linearly related to the natural logarithm of the apparent rate constant, which is also linearly related to the natural logarithm of the specific surface area (SSA), as shown in **(d)**. Replicate (number of replicates, $n = 3$) experiments carried out using EAF in deionized water at 90°C indicate a relative standard deviation of 3% in the final Ca concentration (i.e., after 7 days). The relative standard deviation of triplicate ICP-OES measurements for the same sample is < 3%.

the EAF slag. It indicates that the dissolution rate (not normalized to the surface area) decreases with increasing median particle size d_{50} and decreasing specific surface area (Fig. 2c and d). Specifically, increasing surface area by about a factor of 8 resulted in an approximately three-fold increase in the solution concentration of Ca after 24 h. The lack of a linear relationship between rate (or rate constant) and total surface area can be explained by the nonlinear equivalence in total and reactive surface areas; for example, a power relationship between rate and specific surface area was observed (Fig. 2d), as has been previously observed for feldspars (K-, Al-, Na-, or Ca-rich framework silicates), in which a plateau is observed at high specific surface area (Holdren and Speyer, 1987). This has been explained previously by the dominant control of surface defects on the overall dissolution rate, and their characteristic spacing relative to the particle size (Holdren and Speyer, 1987). For the coarsest size fraction, the defect density is generally constant over a large range of particle sizes because the spacing between two adjacent defects is considerably smaller than the particle size. Hence, a linear relationship between specific surface area and rate is evident. As the particle size decreases, the defect spacing approaches the grain size. Then, decreasing the particle size further does not necessarily result in a corresponding increase in rates. In other words, increasing surface area does not result in a linearly proportional increase in the number of surface defects and dissolution rates.

A similar effect can be envisaged for the relative distributions of reactive sites of phases. Notably, this has previously been shown to prevail for feldspars of grain sizes between 50 and 400 mesh (282 µm–37 µm), a range that is in excellent agreement with our current work. Further decreasing the particle size (and increasing surface area to a larger extent) by grinding did not result in a significant increase in rates. This has been previously explained by the destruction of reaction sites by further grinding (Holdren and Speyer, 1987), a finding that is consistent with our results, considering that the size fraction with d_{50} ~5 µm was ground by hand using an agate mortar and pestle. It is noted that in this set of experiments, the maximum extent of dissolution is at most ~10% by mass of the initial solid, suggesting that the total surface areas did not change significantly over the duration of the experiment. In summary, while the intrinsic dissolution rate of a chemically homogeneous phase is independent of particle size, mechanically ground particles experience fragmentation that not only reduces size but also alters the density of defects and reactive sites. As a result, the dissolution rate may vary with particle size, as observed in this study (Chen et al., 2025; Hidalgo et al., 2022).

Moreover, using α of 0.1 and 0.2 in Eq. (1) for experiments at 25 °C and 90 °C, respectively, we obtained similar trends in the apparent rate constant as a function of particle size (Fig. 2c and d). This supports the idea that the observed rate dependence on particle size is likely a geometrical effect, which does not vary with temperature. These results demonstrate that increasing surface area by grinding, which is associated with a large energy input, does not always result in equivalent enhancements in dissolution rates. Such information is useful when optimizing energy use and the amount of Ca extracted from the solid.

3.2. Effect of reaction conditions and slag type on the kinetics of Ca release

The rates of slag dissolution at three different temperatures (25, 45, and 90°C) in DI water were evaluated under static conditions for the six slag types previously characterized (**Figure S2**). As expected, increasing the temperature from 25 to 90°C increased the rates of Ca release in solution across all slag types. In DI water, which rapidly evolved to a

highly alkaline solution, blast oxygen furnace (BOF) slag featured the most favorable leaching kinetics, whereas air-cooled blast furnace (ac-BF) slag showed the lowest Ca release rate (**Figure S2**). Increasing temperature resulted in increased apparent reaction order, α, from 0.1 at 25°C to 0.2 at 90°C. This suggests a change in the overall control of Ca release, which appears to be a combination of dissolution of primary minerals in the slags and the precipitation of secondary phases. For instance, a higher value of α signifies a faster rate of Ca release and may be caused by the rate of Ca release overcoming precipitation of calcium silicate phases, whose solubility increases with increasing temperature. A characteristic initial increase in Si concentrations (at the first sampling time of 1 h) followed by a gradual decrease, which continued until the end of the experiment, was observed for all slag types except ac-BF slag, in which Si concentrations continued to increase with time (**Figure S3**). This suggests that the presence of Ca (or Mg) and Si in solution resulted in the formation of calcium or magnesium silicate phases, thereby sequestering aqueous Si and Ca (or Mg).

Although the initial bulk Ca content was similar across all slags (Fig. 1c, **Table S3**), the extents of Ca release at a given time differed by up to an order of magnitude. For instance, [Ca] in water reacted with BOF slag reached up to ~10 mM after 24 h, whereas this concentration is only ~1 mM in water reacted with ac-BF slag. The sluggish Ca release rates of ac-BF can be attributed to its high degree of crystallinity, as evidenced by both XRD and petrographic analysis of thin sections revealing large crystal sizes greater than 0.5 mm in length (**Figure S4**). The discrepancies in Ca release can further be attributed to its mineralogy, as discussed below.

To evaluate the effect of pH on dissolution kinetics and for comparison with observations under alkaline conditions, the slags were reacted with 1% and 5% by volume of acetic acid (HOAc) (prepared by adding an appropriate volume of glacial acetic acid (17.4 M) to DI water) at different temperatures. These solutions have initial pH values of 2.78 and 2.38, respectively. The final pH of the 5% acetic acid solutions ranged from 3.9 to 4.0. Under these conditions, substantially higher solution Ca concentrations were obtained, reaching values greater than 60 mM after 24 h (**Figure S5**). Based on PHREEQC (Parkhurst and Appelo, 2013) calculations, adding 10 mM acetate in water does not significantly increase the solubility of Ca, such that the enhancement in rates observed herein was likely caused primarily by pH changes. In addition, considerable amounts of Mg of up to >15 mM were obtained after 24 h. This is in contrast with observations in DI water/-alkaline solutions, in which Mg concentrations were <1 mM even at the highest temperature of 90°C.

The effect of metal complexing agents on Ca release rates was also evaluated from an experiment in 10 mM disodium EDTA solution at 45°C (**Figure S6**). Evidently, the presence of EDTA markedly increased Ca release rates for all slag types, and increased final [Ca] to a lesser extent. The solution reached the final (maximum) [Ca] of about 12 mM within 1 h; [Ca] increased by up to >5 times compared to that at the same temperature, but with no added EDTA. In deionized water, similar concentrations of about 10 mM are reached only after 24 h of reaction. The final pH of the solution generally ranged from 11.4 to 11.8 after 7 days, except for ac-BF, in which the measured pH in the solution with added EDTA is 8.9. Hence, the addition of EDTA primarily affects the rates of Ca release but does not affect its extent significantly.

Another process parameter that is important to consider in carbonation reactions is the ratio of the solid reactant to the reaction solution. The effect of solid-to-liquid ratio (S:L) on the rate and amount of Ca release was also evaluated. The trends of Ca release with time in 1:100 (1 g slag added to 100 g water) and 2:100 S:L are indistinguishable. At even higher S:L (5:100 and 10:100), much higher [Ca] are obtained initially, which gradually decreased over time and then stabilized. All four S:L investigated seem to approach the same value for [Ca], as equilibrium is progressively achieved, suggesting solubility control. A similar observation of a non-straightforward dependence on S:L has been shown previously (De Windt et al., 2011).

It is evident that the processes of dissolution and leaching are accompanied by the formation of precipitates, which were observed directly in most experiments. Solution speciation and the evolution of the saturation indices of pertinent secondary phases can be simulated using PHREEQC using the time-dependent elemental release data from ICP-OES. However, it is important to note that the solution compositions reflect both dissolution and potential precipitation processes, and that the net concentrations are determined by the relative rates and extents of these two processes. Nonetheless, these calculations show that the solution became supersaturated with respect to calcium silicate hydrates. In a previous study (De Windt et al., 2011), phases considered in a similar approach included brucite ($Mg(OH)_2$), chalcedony (SiO_2), C-S-H, diaspore (AlO(OH)), $Fe(OH)_3$, goethite (FeO(OH)), hydrogarnet ($Ca_3Al_2(SiO_4)_{3-x}(OH)_{4x}$), magnetite ($Fe_3O_4$), and portlandite ($Ca(OH)_2$). However, only C-S-H phases were predicted to have relatively fast precipitation kinetics with respect to the leaching duration, and hence precipitate as secondary products during leaching. In fact, C-S-H and ettringite have both been observed in leached BOF slags (De Windt et al., 2011). Hence, it is likely that the *apparent* rate of release of metals at longer times is controlled by the solubility of the secondary precipitates, resulting in a general decrease in rates over time. Hence, both the approach to saturation with respect to primary or secondary phases and the reduction in reactive surface area over time control kinetics.

3.3. Chemical and mineralogical controls on Ca extraction from slags

In addition to the influence of extrinsic processing (solution) conditions on Ca extraction, intrinsic controls on dissolution, pertaining to the reactivity of the solid, are pertinent. Mineral dissolution processes are generally described as being either “surface-controlled” or “transport-controlled”, depending on whether reactions at the solid surface or transport of dissolved ions away from the surface limit dissolution, respectively. Minerals that dissolve slowly are typically considered to have surface-controlled dissolution, whereas minerals that are reactive have dissolution kinetics that is transport-controlled, such that the prevailing flow conditions (e.g., stirring) affect their rates. Although both mechanisms are likely operating simultaneously, the dominant mechanism can be inferred from the comparison of rates under static and stirred conditions (**Figure S7**). In EAF and ac-BF, the initial rate of Ca release (<1 h) increased upon stirring; thereafter, the *rates* became comparable to those obtained for unstirred conditions. In SS and LS, the rates are indistinguishable from each other, featuring perhaps a slight increase upon stirring initially. In BOF, the initial rates within 6 h of reaction were higher under stirred conditions, whereas apparent Ca release extents at later times were lower than in static conditions. Finally, for cm-EAF, initial rates increased substantially, and the curves corresponding to stirred and unstirred conditions began to converge. In cases wherein stirring increased initial but not final rates, it can be inferred that the overall dissolution kinetics are controlled by an initially transport-controlled and a later surface-controlled process, corresponding to the reaction of fast and slowly dissolving minerals or reactive sites, respectively, as in EAF and ac-BF (see **Figures S7a** and **S7c**). Correspondence of the two curves as in SS and LS implies surface control, i.e., lack of stirring effect (**Figures S7e** and **S7f**), whereas convergence to the same [Ca] signifies steady state (i.e., wherein dissolution and precipitation rates of Ca-containing phases match), as in the fast-reacting BOF and cm-EAF (**Figures S7b** and **S7d**). The differences in overall reactivity and dissolution controls can be attributed to the specific mineral phases contained in each, which have distinct dissolution rates controlled by their composition and crystallographic structure. For instance, BOF slag reacted with water for 7 days was characterized by using XRD to qualitatively assess the changes in its mineralogical make-up. The diffraction peaks corresponding to the highly reactive β-C_2S phase progressively diminished with increasing dissolution extent (simulated by decreasing the pH from 7, 3, and 1), indicating the phase’s preferential dissolution.

Slags are composed of Ca, Mg, and Fe silicates and oxides of varying compositions and structures. There is sparse data on the dissolution kinetics of slag-forming minerals, but their relative reactivities can be inferred from observations of analogous rock-forming minerals. The Ca-containing phases in slags can be separated into 3 types: $Ca(OH)_2$, Ca-(Fe)-silicates, and Ca-Fe-O (Huijgen and Comans, 2005), and Ca and Fe oxides are generally more reactive than their silicate counterparts. Because Si–O hydrolysis is a primary step in the dissolution of silicate minerals, the reactivity of silicates is generally controlled by the connectivity of their silica tetrahedral structure, i.e., the degree of polymerization which arises when the solid crystallizes from a silicate melt (Stumm and Morgan, 2012). The silica tetrahedra building blocks of silicates may be isolated, as in nesosilicates, having Si:O molar ratio of 1:4, form pairs as in sorosilicates (Si:O = 2:7), connected in chains as in inosilicates (Si:O = 1:3 or 4:11), arrange in sheets as in phyllosilicates (Si:O = 2:5) or form a framework, as in tectosilicates (Si:O = 1:2) (**Table S2**). Thus, the degree of polymerization is reflected in the molar amounts of Si relative to the other elements present, such that higher values indicate higher connectivity. Indeed, it can be seen that rate constants obtained from the data shown in **Figure S2** correlate with the Ca/Si ratio, but not with bulk Ca content (Fig. 3a and b). This shows that for solids having similar Ca contents, as in the slags investigated herein: e.g., ac-BF which is ~60% crystalline having melilite as the major phase, and BOF is ~30% crystalline with multiple faster-dissolving minerals such as larnite, it is not the total Ca that controls relative differences in rates of Ca extraction in water, but instead the fraction of Ca that is present in the reactive (less polymerized) phases (see **Figures S2, 4**, and **5**).

The increase in dissolution rate in acidic compared to alkaline conditions can be explained by the pH-dependent rates of dissolution of the various phases in the slags, as previously shown empirically (Engström et al., 2013; Hall et al., 2014; Strandkvist et al., 2015). For instance, Mg-containing Ca-silicates dissolve appreciably only at low pH. Under alkaline conditions, BOF slag, which is composed primarily of Ca-silicates/-aluminates, exhibited the highest rates of Ca release. On the other hand, SS and LS slags, composed of Ca-Mg-, and Ca-F- silicates containing the highest bulk Ca, dissolved fastest under acidic pH conditions. This is because the dissolution rates of Ca-Al-silicate, Ca-F-silicate, and Ca-Mg-silicate are more significantly enhanced in acidic conditions compared to C_2S (Engström et al., 2013; Inoue and Suito, 2002). The dissolution rates of the isochemical phases β-C_2S and γ-C_2S have been shown not to depend strongly on pH over the range of 4–10 (Strandkvist et al., 2015). In addition, the dissolution rate of calcite, abundant in SS and LS but not in BOF, increases significantly with decreasing pH (Inoue and Suito, 2002).

Hence, under acidic conditions, the composition of the slag becomes a significant determining factor of Ca extractability, in addition to its structure (Fig. 3c). The abundance of cuspidine ($Ca_4F_2SiO_7$) in SS and LS (**Table S2**) is due to the addition of fluorite (CaF_2) during steelmaking in order to increase the solubility of CaO. Dissolution of cuspidine releases small amounts of F^- ions, forming aqueous HF^0 complexes under highly acidic conditions, which may further promote silicate dissolution. This explains the divergence of SS and LS slags from the rate-Ca/Si trend (Fig. 3c). These findings demonstrate that the optimal choice of slag depends on the pH of the reacting solution.

3.4. Rapid and large Ca extraction for utilization at scale

Building on the mineralogical influences and mechanistic insights discussed above, this section investigates the extent of calcium yield expected under high solid loadings, with an emphasis on scalability. It also considers the increased secondary precipitation that occurs alongside dissolution, framed within a dissolution–precipitation kinetic model. Efficient resource recovery through the upcycling of industrial byproducts for broad applications such as large-scale CO_2 mineralization using slags, depends on the rapid, high-throughput solubilization of alkaline earth metals. As explored in this work and other studies (Mei et al., 2022; Doucet, 2010; Ragipani et al., 2020), the composition and mineral structure of slags are key intrinsic factors dictating both the speed and extent of dissolution and metal-leaching (**Figure S2** and Section 3.3). In contrast, extrinsic factors are primarily related to interfacial reaction kinetics and the surrounding ion transport mechanisms, including both diffusion and advection in aqueous media (**Figures S2** and **S7**). Operating under dilute conditions increases water use and wastewater generation. Additionally, while external heating may enhance apparent dissolution (**Figure S2**), it incurs high energy costs because of water's high specific heat capacity. Similarly, excessive grinding of feedstock may not significantly improve dissolution efficiency (Fig. 2a and b), yet it contributes to increased energy demand.

Therefore, an effective approach involves reacting slags with either organic or strong inorganic acids at high S:L ratios under ambient temperature and pressure, using moderately fine particles. This promotes rapid proton attack on Ca-bearing minerals, facilitating substantial Ca^{2+} mobilization. However, this also leads to the release of other ions (**Figure S3**), which can co-precipitate with target metals into more thermodynamically stable secondary phases. This shifts the system to a precipitation-controlled regime, including passivation effects (Mei et al., 2022; Zhang et al., 2013; Said et al., 2015).

To evaluate mineralogical contrasts, two slags, ac-BF and BOF, were selected based on their similar calcium content with differing crystallographic structures. These differences result in markedly distinct Ca release rates in water, representing the upper and lower bounds of the dissolution envelope depicted in **Figure S2**. Fig. 4 shows the Ca solubilization yield from reactions involving BOF and ac-BF slags (106-150 μm particle size) at an S:L = 1:10 under conditions of unrestricted proton availability (i.e., buffered with HNO_3) across a controlled pH range from 1 to 12 with constant stirring. Here, Ca solubilization yield is defined as the concentration of dissolved Ca measured at a given time. Overall,

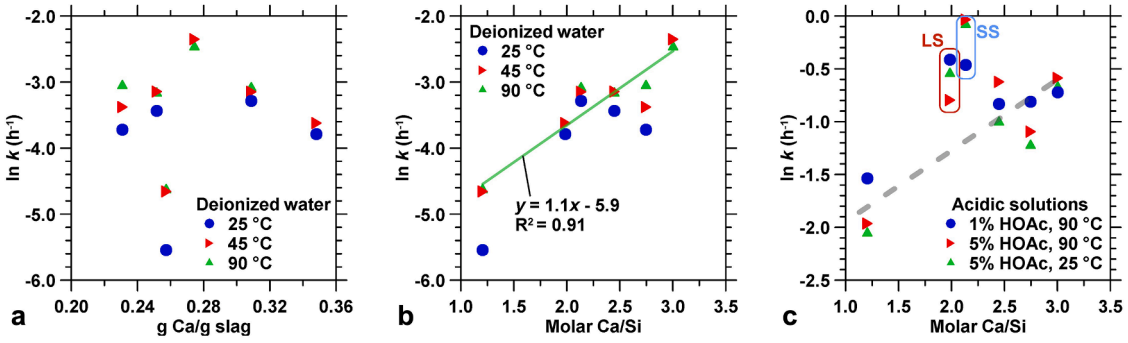

Fig. 3. Natural logarithm of rate constant as a function of **(a)** mass of Ca per unit mass of slag, and **(b), (c)** molar Ca/Si ratio of the slag, in **(b)** deionized water (i.e., under alkaline conditions), and **(c)** under acidic conditions. The green line in **(b)** shows the best-fit line for the data obtained at 90°C, whereas the dashed gray line in **(c)** is drawn to guide the eye to show the relationship between ln *k* and molar Ca/Si while excluding the data points corresponding to stainless steel and ladle slags.

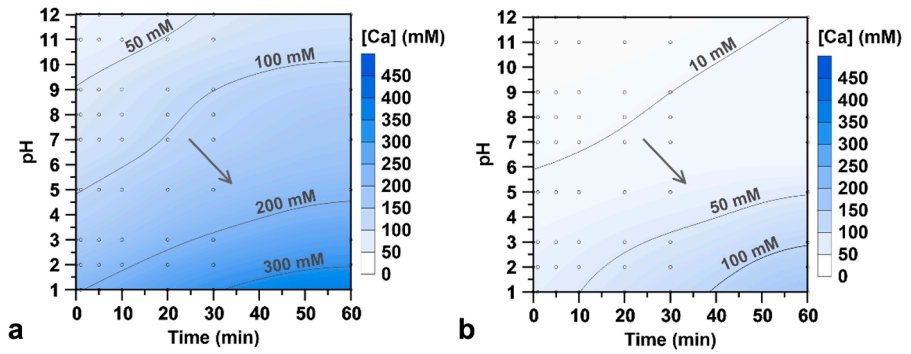

Fig. 4. Ca solubilization yield in 1-hour pH-controlled dissolution at an S:L of 1:10 using 106-150 μm particles of **(a)** BOF and **(b)** ac-BF slags. Duplicate experiments were performed for representative conditions (pH 1, 3, and 7), where the average percentage deviations in measured Ca concentration (mM), Ca and bulk slag dissolved fraction (%), and molar Ca/Si ratio did not exceed 7% for BOF and 18% for ac-BF.

[Ca] increased over time and with decreasing pH. At pH 1 after 1 h, BOF slag solubilized ~440 mM of Ca, while the ac-BF yielded ~220 mM of Ca. Notably, for BOF, about half of the 1-hour Ca concentration was reached within <5 min, whereas ac-BF required about 20 min to reach the same proportion, regardless of pH. Across all pH conditions and time points, BOF consistently released at least twice as much Ca compared to ac-BF, and in some cases, up to an order of magnitude more. This rapid release is attributed to a significant mass fraction of Ca present in amorphous phases (~40% of the total Ca in the BOF slag), as well as to fast-dissolving crystalline phases present, as evidenced more clearly under dilute conditions (Fig. 6d). These results highlight significant differences in both acid consumption and time required to reach target Ca concentrations between the two slags. This underscores the importance of slag cooling methods; rapid quenching during production yields slags with more reactive mineral phases, thereby enabling more efficient Ca mobilization for downstream applications.

To incorporate the effects of re-/co-precipitation in the dissolution kinetics of slags at high S:L, a semi-empirical two-parameter model was used:

$$X_{Ca} = \frac{k_0}{k_1}\left(1 - e^{-k_1 t}\right) \quad (2)$$

where k_0 is the zero-order dissolution parameter (mM/min), k_1 is the first-order precipitation parameter (min^{-1}), and t is the time (min).

Fig. 5 shows the Ca solubilization rate for BOF and ac-BF slags under fixed pHs in acidic-to-neutral environments (pH 1, 3, and 7). BOF slag exhibited a rapid initial release of Ca within the first 2 min, followed by a marked shift at around 5 min to a slower, more gradual rate beyond 10 min. In contrast, ac-BF showed more gradual changes in dissolution rates throughout (Fig. 5a). The fraction of Ca solubilized relative to the total Ca content in the unreacted slags in substantial, e.g., nearly 6% for BOF and 30% for ac-BF at pH 1 after 1 h. The dissolution parameter, k_0, decreases systematically with decreasing acidity for both slags, decaying approximately linearly with increasing $[H^+]$ for BOF and with increasing pH for ac-BF (Fig. 5b). The precipitation parameter, k_1, for BOF decreases linearly with decreasing acidity, while for ac-BF, it increases with pH and then plateaus, reflecting reduced dissolution and consequently less secondary precipitation (Fig. 5c). Overall, both k_0 and k_1 are significantly higher for BOF, consistent with its higher reactivity.

The Ca-bearing phases identified in Fig. 5a are significantly more reactive than the overall bulk composition of the slags (Fig. 6a and b). As discussed in Section 3.3, the proportion of Ca associated with reactive, less polymerized phases governs the dissolution rate. In ac-BF, both the total dissolved fraction and Ca solubilization are primarily influenced by the breakdown of melilite (akermanite), which features a higher degree of polymerization.

Compared to Si solubilization, Ca release spikes rapidly at early stages due to the presence of readily soluble phases such as carbonates and hydrates, followed by aluminates (Fig. 6c). After approximately 10 min, the molar Ca/Si ratio in solution stabilizes and becomes roughly proportional, a trend also observed for magnesium and aluminum, which co-occur within the melilite solid solution. For BOF slag, the molar Ca/Si ratio remains nearly proportional throughout the reaction period. However, this proportionality is less consistent for elements like Mg, Fe, and Al due to the concurrent dissolution and secondary precipitation of multiple mineral phases. The Ca-silicate phases in BOF (mainly larnite) contain fewer and less polymerized silicate groups than melilite, making them more reactive under highly acidic conditions (pH 1), as implied by a Ca/Si ratio near 1. At milder acidity (pH 3), the [Ca] in solution remains nearly twice that of [Si]. These observations provide mineralogy-specific insights into the apparent rates and extents of Ca solubilization under precipitation-controlled conditions, offering a pathway to optimize slag utilization for large-scale applications.

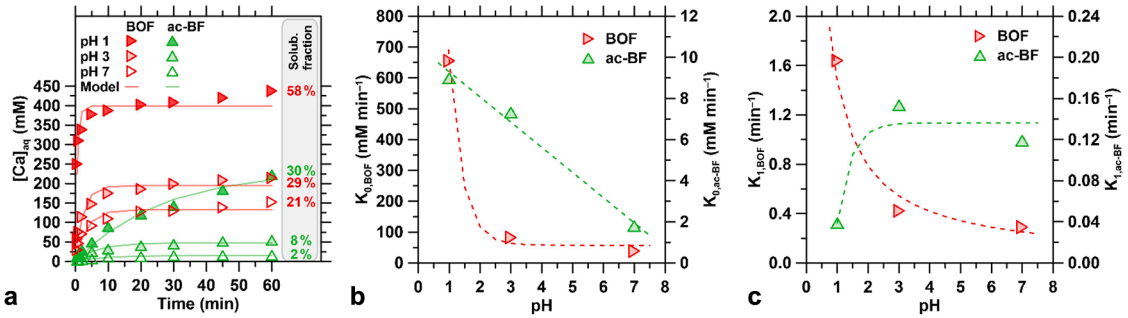

Fig. 5. Ca dissolution and precipitation kinetics ($n = 2$): **(a)** Experimental and modeled fits showing Ca solubilization yield and fraction (on a molar basis) over 1 hour under pH-controlled conditions for BOF and ac-BF slags (106–150 μm particle size) at an S:L ratio of 1:10 across acidic to neutral pH; **(b)** zero-order dissolution rate constants, k_0, and **(c)** first-order precipitation rate constants, k_1, derived from the kinetic model.

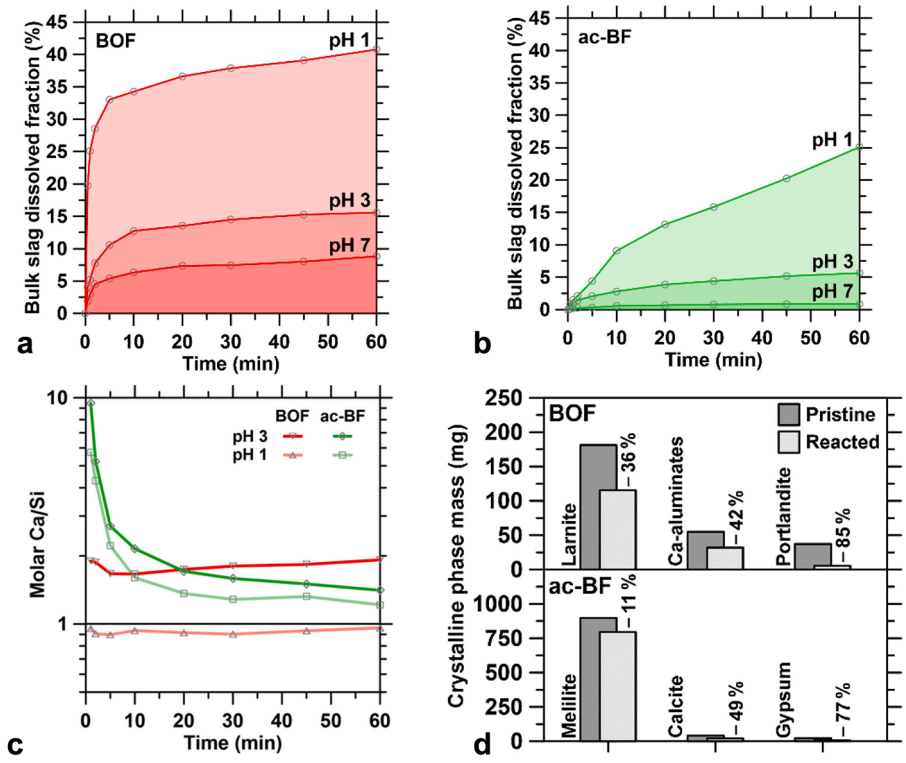

Fig. 6. Bulk slag dissolved fraction under pH-controlled dissolution at an S:L of 1:10 with 106–150 μm particles over 1 h for **(a)** BOF and **(b)** ac-BF slags, and **(c)** their corresponding bulk Ca/Si molar ratios. ($n = 2$) **(d)** Dissolution of the primary Ca-bearing crystalline phases estimated via Rietveld refinement from free pH drift batch experiments initiated at pH 7 under highly dilute conditions (S:L = 1:2500) using BOF and ac-BF slags with 106-150 μm particle size. ($n = 1$).

4. General implications on CO_2 mineralization

The findings of this study offer valuable insights for optimizing CO_2 mineralization processes that rely on calcium extraction via dissolution from slags and other alkaline solids. We quantified the extent of Ca extraction enhancement as a function of temperature and demonstrated the influence of stirring on rates. This is particularly relevant, as stirring within leaching reactors is a major contributor to the overall energy consumption in carbonation systems, especially for prolonged reactions, at high-solid loadings, and over periods spanning several days. For solids with primarily surface-controlled dissolution, such as EAF and ac-BF slags, stirring was found to accelerate Ca release only during the initial hour. This likely reflects enhanced mass transfer during the early dissolution of highly reactive phases. Practically, this suggests that, to optimize energy use while maximizing Ca recovery under dilute conditions, stirring should be limited to the early stages of reaction. Beyond the first hour, its impact on kinetics becomes negligible. In contrast, for SS and LS slags, where surface-controlled dissolution dominates, stirring had little to no effect on the release rates.

By correlating Ca release rates under various processing conditions with slag mineralogy and composition, this study helps identify the solid-state properties that render slags more suitable for carbonation. Importantly, the extent of carbonation is closely linked to the amount of Ca that can be solubilized, not just the total Ca content, but also the specific mineral phases that host it. This distinction is critical in crystalline materials like slags, where individual phases show markedly different reactivities. Furthermore, since different minerals exhibit variable pH-dependencies in their dissolution rates, slag selection can be tailored based on the pH conditions of the carbonation process. For example, SS and LS slags rich in γ-C_2S, cuspidine, and calcite outperformed BOF slag in reactions with organic acids under dilute conditions. Conversely, BOF slag exhibited superior performance in alkaline environments due to its high reactivity across a broader pH range.

Large-scale application is feasible given the substantial Ca mobilization achieved under high solid-to-liquid (S:L) ratios with unrestricted acid supply. For instance, in slags containing ~25–30 wt% Ca and differing in crystalline structure and silicate polymerization (e.g., BOF and ac-BF), ~30–60% of their calcium were solubilized within 1 h when reacted with inorganic acid buffered to pH 1. This level of extraction could theoretically support CO_2 uptake of ~0.1–0.2 tonnes of CO_2 per tonne of slag. Additionally, the co-dissolution of magnesium (~20–40%) can further boost CO_2 sequestration potential (Chu et al., 2019). Furthermore, longer reaction times, more aggressive acidic environments (Hong et al., 2021), or enhanced weathering over extended periods (Hartmann et al., 2013) also offer avenues to increase total carbonation potential. Kinetic measurements under controlled laboratory conditions provide estimates for industrial CO_2 mineralization, which is further influenced by mass transfer and the characteristics of industrial CO_2 streams, among others (Liu et al., 2021; Liu et al., 2026). In summary, these results underscore the strong potential for rapid resource recovery and large-scale CO_2 mineralization using slags, especially when mineralogical and operational factors are carefully tuned.

5. Summary and conclusions

This study systematically quantified the rates and extents of calcium extraction from a wide range of crystalline slag types. By correlating Ca release kinetics with in-depth chemical and mineralogical characterization, we established clear links between slag composition and dissolution behavior. In dilute systems, dissolution followed a power-law dependence over time, allowing for the determination of apparent rate constants and reaction orders and facilitating direct comparisons across slag types and process conditions. Additionally, we investigated precipitation-controlled kinetics under conditions that promote rapid and extensive Ca solubilization. A key finding is that Ca extractability is not solely dictated by the total calcium content of the slag but is strongly influenced by the specific mineral phases present. The critical role of

slag mineralogy, particularly the silicate structure of constituent phases, was shown to govern reactivity far more than bulk composition alone. These insights offer a pathway to optimize slag selection and processing strategies for targeted applications, with implications that extend to other crystalline solids. Importantly, the ability to rapidly mobilize substantial quantities of Ca positions these slags as promising feedstocks for scalable CO_2 mineralization technologies, contributing to climate change mitigation through effective carbon capture and utilization.

CRediT authorship contribution statement

Erika La Plante: Writing – original draft, Visualization, Methodology, Investigation, Funding acquisition, Formal analysis, Conceptualization. **Adriano Leão:** Writing – review & editing, Visualization, Methodology, Investigation, Formal analysis, Conceptualization. **Micah Bob:** Investigation, Formal analysis. **Yi-Hsuan Hsiao:** Investigation, Formal analysis. **Owen Daily:** Investigation, Formal analysis. **Gwenn Le Saout:** Investigation, Formal analysis. **Laurent Pilon:** Writing – review & editing, Supervision, Funding acquisition, Formal analysis, Conceptualization. **Gaurav N. Sant:** Writing – review & editing, Supervision, Funding acquisition, Formal analysis, Conceptualization.

Declaration of competing interest

The authors declare that they have no known competing financial interests or personal relationships that could have appeared to influence the work reported in this paper.

Acknowledgements

The authors acknowledge financial support for this research from the: United States, Department of Energy, Office of Fossil Energy via the National Energy Technology Laboratory (NETL) (DE-FE0029825), United States Department of Energy, Advanced Research Projects Agency-Energy (ARPA-E: DE-AR00017777) and the National Science Foundation (CAREER Award #2342381). This research was conducted in: Laboratory for the Chemistry of Construction Materials (LC^2) at the University of California, Los Angeles and the Materials Chemistry Laboratory (MCL) and the Peter A. Rock Thermochemistry Laboratory at the University of California, Davis. As such, the authors gratefully acknowledge the support that has made these laboratories and their operations possible. The contents of this paper reflect the views and opinions of the authors, who are responsible for the accuracy of the datasets presented herein, and do not reflect the views and/or policies of the funding agencies, nor do the contents constitute a specification, standard or regulation.

Data availability

Data will be made available on request.

References

Bobicki, E.R., Liu, Q., Xu, Z., Zeng, H., 2012. Carbon capture and storage using alkaline industrial wastes. Prog. Energy Combust. Sci. 38 (2), 302–320. https://doi.org/10.1016/j.pecs.2011.11.002.

Chang, E.-E., Chiu, A.-C., Pan, S.-Y., Chen, Y.-H., Tan, C.-S., Chiang, P.-C., 2013. Carbonation of basic oxygen furnace slag with metalworking wastewater in a slurry reactor. Int. J. Greenh. Gas Control 12, 382–389. https://doi.org/10.1016/j.ijggc.2012.11.026.

Chen, Z., Liu, Y., Sui, H., Souza, F.B.D., Sagoe-Crentsil, K., Neild, A., Duan, W., 2025. Investigating tricalcium silicate dissolution kinetics in cementitious materials through single-particle analysis. J. Am. Ceram. Soc. 108 (7), e20491. https://doi.org/10.1111/jace.20491.

Christian, J.W., 2002. The Theory of Transformations in Metals and Alloys. Newnes.

Chu, G., Li, C., Liu, W., Zhang, G., Yue, H., Liang, B., Wang, Y., Luo, D., 2019. Facile and cost-efficient indirect carbonation of blast furnace slag with multiple high value-added products through a completely wet process. Energy 166, 1314–1322. https://doi.org/10.1016/j.energy.2018.10.128.

De Windt, L., Chaurand, P., Rose, J., 2011. Kinetics of steel slag leaching: batch tests and modeling. Waste Manag. 31 (2), 225–235. https://doi.org/10.1016/j.wasman.2010.05.018.

DiGiovanni, C., Hisseine, O.A., Awolayo, A.N., 2024. Carbon dioxide sequestration through steel slag carbonation: review of mechanisms, process parameters, and cleaner upcycling pathways. J. CO_2 Util. 81, 102736. https://doi.org/10.1016/j.jcou.2024.102736.

Doucet, F.J., 2010. Effective CO2-specific sequestration capacity of steel slags and variability in their leaching behaviour in view of industrial mineral carbonation. Miner. Eng. 23 (3), 262–269. https://doi.org/10.1016/j.mineng.2009.09.006.

Dri, M., Sanna, A., Maroto-Valer, M.M., 2013. Dissolution of steel slag and recycled concrete aggregate in ammonium bisulphate for CO2 mineral carbonation. Fuel Process. Technol. 113, 114–122. https://doi.org/10.1016/j.fuproc.2013.03.034.

Dutta, S.K., Chokshi, Y.B., 2020. Basic Concepts of Iron and Steel Making. Springer Singapore, Singapore. https://doi.org/10.1007/978-981-15-2437-0.

Engström, F., Adolfsson, D., Samuelsson, C., Sandström, Å., Björkman, B., 2013. A study of the solubility of pure slag minerals. Miner. Eng. 41 (Supplement C), 46–52. https://doi.org/10.1016/j.mineng.2012.10.004.

Franke, M.D., Ernst, W.R., Myerson, A.S., 1987. Kinetics of dissolution of alumina in acidic solution. AIChE J. 33 (2), 267–273. https://doi.org/10.1002/aic.690330213.

Gautier, J.-M., Oelkers, E.H., Schott, J., 2001. Are quartz dissolution rates proportional to B.E.T. Surface areas? Geochim. Cosmochim. Acta 65 (7), 1059–1070. https://doi.org/10.1016/S0016-7037(00)00570-6.

Gbor, P.K., Jia, C.Q., 2004. Critical evaluation of coupling particle size distribution with the shrinking core model. Chem. Eng. Sci. 59 (10), 1979–1987. https://doi.org/10.1016/j.ces.2004.01.047.

Grubeša, I.N., Barišic, I., 2021. CHAPTER 7. Diverse applications of slags in the construction industry. In: Piatak, N.M., Ettler, V. (Eds.), Chemistry in the Environment. Royal Society of Chemistry: Cambridge, pp. 194–233. https://doi.org/10.1039/9781839164576-00194.

Guo, J., Bao, Y., Wang, M., 2018. Steel slag in China: treatment, recycling, and management. Waste Manag. 78, 318–330. https://doi.org/10.1016/j.wasman.2018.04.045.

Hall, C., Large, D.J., Adderley, B., West, H.M., 2014. Calcium leaching from waste steelmaking slag: significance of leachate chemistry and effects on slag grain mineralogy. Miner. Eng. 65 (Supplement C), 156–162. https://doi.org/10.1016/j.mineng.2014.06.002.

Hartmann, J., West, A.J., Renforth, P., Köhler, P., De La Rocha, C.L., Wolf-Gladrow, D.A., Dürr, H.H., Scheffran, J., 2013. Enhanced chemical weathering as a geoengineering strategy to reduce atmospheric carbon dioxide, supply nutrients, and mitigate ocean acidification. Rev. Geophys. 51 (2), 113–149. https://doi.org/10.1002/rog.20004.

Hidalgo, J., Roussel, P., Okuno, H., Delahaye, T., Rouvière, J.L., Leturcq, G., 2022. Influence of milling on structural and microstructural properties of cerium oxide: consequence of the surface activation on the dissolution kinetics in nitric acid. Hydrometallurgy 207, 105774. https://doi.org/10.1016/j.hydromet.2021.105774.

Holdren, G.R., Speyer, P.M., 1987. Reaction rate-surface area relationships during the early stages of weathering. II. Data on eight additional feldspars. Geochim. Cosmochim. Acta 51 (9), 2311–2318. https://doi.org/10.1016/0016-7037(87)90284-5.

Hong, S., Park, A.-H.A., Park, Y., 2021. Evaluation of elemental leaching behavior and morphological changes of steel slag in both acidic and basic conditions for carbon sequestration potential. Korean J. Chem. Eng. 38 (11), 2279–2285. https://doi.org/10.1007/s11814-021-0874-5.

Hosseini, T., Selomulya, C., Haque, N., Zhang, L., 2014. Indirect carbonation of victorian brown coal fly ash for CO2 sequestration: multiple-cycle leaching-carbonation and magnesium leaching kinetic modeling. Energy Fuels 28 (10), 6481–6493. https://doi.org/10.1021/ef5014314.

Huijgen, W.J.J., Comans, R.N.J., 2003. Carbon Dioxide Sequestration By Mineral Carbonation. Literature Review. Energy research Centre of the Netherlands ECN. ECN-C–03-016. http://inis.iaea.org/Search/search.aspx?orig_q=RN:34066562 (accessed 2017-11-13).

Huijgen, W.J.J., Comans, R.N.J., 2005. Mineral CO2 sequestration by steel slag carbonation. Environ. Sci. Technol. 39 (24), 9676–9682. https://doi.org/10.1021/es050795f.

Huijgen, W.J.J., Comans, R.N.J., 2006. Carbonation of steel slag for CO2 sequestration: leaching of products and reaction mechanisms. Environ. Sci. Technol. 40 (8), 2790–2796. https://doi.org/10.1021/es052534b.

Hulbert, S.F., 1970. Kinetics of alumina removal from a calcined kaolin with nitric, sulphuric and hydrochloric acids. Clay Miner. 8 (3), 337–345. https://doi.org/10.1180/claymin.1970.008.3.11.

Inoue, R., Suito, H., 2002. Fluorine-containing mineral phases in ironmaking and steelmaking slags and their solubilities in aqueous solution. ISIJ Int. 42 (7), 785–793. https://doi.org/10.2355/isijinternational.42.785.

International Energy Agency, 2021. Iron and steel technology roadmap: towards more sustainable steelmaking. https://iea.blob.core.windows.net/assets/eb0c8ec1-3665-4959-97d0-187ceca189a8/Iron_and_Steel_Technology_Roadmap.pdf (accessed 2025-03-30).

Kirchofer, A., Brandt, A., Krevor, S., Prigiobbe, V., Becker, A., Wilcox, J., 2013. Assessing the potential of mineral carbonation with industrial alkalinity sources in the U.S. Energy Procedia 37 (Supplement C), 5858–5869. https://doi.org/10.1016/j.egypro.2013.06.510.

Kokko, M., Kauppinen, T., Hu, T., Tanskanen, P., Kallio, R., Lassi, U., Pesonen, J., 2024. Two-stage leaching of calcium and vanadium from high-calcium steelmaking slag. Environ. Technol. 45 (27), 5966–5981. https://doi.org/10.1080/09593330.2024.2316671.

Kumar, D., Kumar, D., 2015. Management of Coking Coal Resources. Elsevier Ltd, Amsterdam.
Leão, A.S., Medeiros, D.L., Santiago, M.A., Do Carmo Tavares, A.O., Maranduba, H.L., Almeida, E.D.S, 2023. Rigorous environmental and energy life cycle assessment of blast furnace pig iron in Brazil: the role of carbon and iron sources, and co-product utilization. Sustain. Mater. Technol. 36, e00607. https://doi.org/10.1016/j.susmat.2023.e00607.
Leão, A.S., Tavares, A.D.C., Maranduba, H.L., Almeida, E.D.S., 2020. Environmental assessment of pig iron production: systematic review of literature, bibliometrics and patents. Rev. Bras. Gest. Ambient. E Sustentabilidade 7 (16), 905–936. https://doi.org/10.21438/rbgas(2020)071629.
Lekakh, S.N., Rawlins, C.H., Robertson, D.G.C., Richards, V.L., Peaslee, K.D., 2008. Kinetics of aqueous leaching and carbonization of steelmaking slag. Metall. Mater. Trans. B 39 (1), 125–134. https://doi.org/10.1007/s11663-007-9112-8.
Li, L., Ling, T.-C., Pan, S.-Y., 2022. Environmental benefit Assessment of steel slag utilization and carbonation: a systematic review. Sci. Total Environ. 806, 150280. https://doi.org/10.1016/j.scitotenv.2021.150280.
Li, Y., Liao, H., Guo, Y., 2025. Aqueous carbonation of steel slag and preparation of calcium carbon: a new strategy for the utilization of steel slag. J. Environ. Chem. Eng. 13 (2), 115951. https://doi.org/10.1016/j.jece.2025.115951.
Liu, W., Teng, L., Rohani, S., Qin, Z., Zhao, B., Xu, C.C., Ren, S., Liu, Q., Liang, B., 2021. CO2 Mineral carbonation using industrial solid wastes: a review of recent developments. Chem. Eng. J. 416, 129093. https://doi.org/10.1016/j.cej.2021.129093.
Liu, X., Ai, X., Que, Z., Liu, X., Zhang, Z., 2026. A review of steel slag carbonation: mechanisms, applications, and sustainability assessment. Materials 19 (2), 286. https://doi.org/10.3390/ma19020286.
Mei, X., Zhao, Q., Min, Y., Liu, C., Saxén, H., Zevenhoven, R., 2022. Phase transition and dissolution behavior of Ca/Mg-bearing silicates of steel slag in acidic solutions for integration with carbon sequestration. Process Saf. Environ. Prot. 159, 221–231. https://doi.org/10.1016/j.psep.2021.12.062.
Montes-Hernandez, G., Pérez-López, R., Renard, F., Nieto, J.M., Charlet, L., 2009. Mineral sequestration of CO2 by aqueous carbonation of coal combustion fly-ash. J. Hazard. Mater. 161 (2), 1347–1354. https://doi.org/10.1016/j.jhazmat.2008.04.104.
Moon, S., Kim, E., Noh, S., Triwigati, P.T., Choi, S., Park, Y., 2024. Carbon mineralization of steel and iron-making slag: paving the way for a sustainable and carbon-neutral future. J. Environ. Chem. Eng. 12 (2), 112448. https://doi.org/10.1016/j.jece.2024.112448.
Nikolić, I., Drinčić, A., Djurović, D., Karanović, L., Radmilović, V.V., Radmilović, V.R., 2016. Kinetics of electric arc furnace slag leaching in alkaline solutions. Constr. Build. Mater. 108, 1–9. https://doi.org/10.1016/j.conbuildmat.2016.01.038.
Olmez, G.M., Dilek, F.B., Karanfil, T., Yetis, U., 2016. The environmental impacts of iron and steel industry: a life cycle assessment study. J. Clean. Prod. 130, 195–201. https://doi.org/10.1016/j.jclepro.2015.09.139.
Parkhurst, D.L., Appelo, C.A.J., 2013. Description of input and examples for PHREEQC version 3—A computer program for speciation, batch-reaction, one-dimensional transport, and inverse geochemical calculations. US Geol. Surv. Tech. Methods Book 6, 497.
Pecina, T., Franco, T., Castillo, P., Orrantia, E., 2008. Leaching of a zinc concentrate in H2SO4 solutions containing H2O2 and complexing agents. Miner. Eng. 21 (1), 23–30. https://doi.org/10.1016/j.mineng.2007.07.006.
Piatak, N.M., Parsons, M.B., Seal, R.R., 2015. Characteristics and environmental aspects of slag: a review. Appl. Geochem. 57, 236–266. https://doi.org/10.1016/j.apgeochem.2014.04.009.
Ragipani, R., Bhattacharya, S., Akkihebbal, S.K., 2020. Understanding dissolution characteristics of steel slag for resource recovery. Waste Manag. 117, 179–187. https://doi.org/10.1016/j.wasman.2020.08.008.
Reeves, D., Rothman, D.H., 2013. Age dependence of mineral dissolution and precipitation rates. Glob. Biogeochem. Cycles 27 (3), 906–919. https://doi.org/10.1002/gbc.20082.
Best Available Techniques (BAT), Europäische Kommission, 2013. In: Remus, R. (Ed.), Reference Document for Iron and Steel Production: Industrial Emissions Directive 2010/75/EU: Integrated Pollution Prevention and Control$Nelektronische Ressource. EUR; Publications Office of the European Union, Luxembourg. https://doi.org/10.2791/97469.
Renforth, P., Washbourne, C.-L., Taylder, J., Manning, D.A.C., 2011. Silicate production and availability for mineral carbonation. Environ. Sci. Technol. 45 (6), 2035–2041. https://doi.org/10.1021/es103241w.
Said, A., Mattila, O., Eloneva, S., Järvinen, M., 2015. Enhancement of calcium dissolution from steel slag by ultrasound. Chem. Eng. Process. Process Intensif. 89, 1–8. https://doi.org/10.1016/j.cep.2014.12.008.
Strandkvist, I., Björkman, B., Engström, F., 2015. Synthesis and dissolution of slag minerals - a study of β-dicalcium silicate, pseudowollastonite and monticellite. Can. Metall. Q. 54 (4), 446–454. https://doi.org/10.1179/1879139515Y.0000000022.
Stumm, W., Morgan, J.J., 2012. Aquatic Chemistry: Chemical Equilibria and Rates in Natural Waters. John Wiley & Sons, p. 126.
Teo, P.T., Zakaria, S.K., Salleh, S.Z., Taib, M.A.A., Mohd Sharif, N., Abu Seman, A., Mohamed, J.J., Yusoff, M., Yusoff, A.H., Mohamad, M., Masri, M.N., Mamat, S., 2020. Assessment of electric arc furnace (EAF) steel slag waste's recycling options into value added green products: a review. Metals 10 (10), 1347. https://doi.org/10.3390/met10101347.
Vogl, V., Åhman, M., Nilsson, L.J., 2021. The making of green steel in the EU: a policy evaluation for the early commercialization phase. Clim. Policy 21 (1), 78–92. https://doi.org/10.1080/14693062.2020.1803040.
Wang, J., Zhong, M., Wu, P., Wen, S., Huang, L., Ning, P., 2021. A review of the application of steel slag in CO_2 fixation. ChemBioEng Rev 8 (3), 189–199. https://doi.org/10.1002/cben.202000021.
Yagi, S., Kunii, D., 1955. Studies on combustion of carbon particles in flames and fluidized beds. Symp. Int. Combust. 5 (1), 231–244. https://doi.org/10.1016/S0082-0784(55)80033-1.
Yildirim, I.Z., Prezzi, M., 2011. Chemical, mineralogical, and morphological properties of steel slag. Adv. Civ. Eng. (1), 463638. https://doi.org/10.1155/2011/463638.
Zhang, H., Xu, A., He, D., Cui, J., 2013. Alkaline extraction characteristics of steelmaking slag batch in NH4Cl solution under environmental pressure. J. Cent. South Univ. 20 (6), 1482–1489. https://doi.org/10.1007/s11771-013-1638-0.
Zhao, Q., Li, J., You, K., Liu, C., 2020. Recovery of calcium and magnesium bearing phases from iron– and steelmaking slag for CO2 sequestration. Process Saf. Environ. Prot. 135, 81–90. https://doi.org/10.1016/j.psep.2019.12.012.
Zhao, Q., Liu, C., Gao, T., Gao, L., Saxén, H., Zevenhoven, R., 2019. Remediation of stainless steel slag with MnO for CO2 mineralization. Process Saf. Environ. Prot. 127, 1–8. https://doi.org/10.1016/j.psep.2019.04.025.